

Amino Acid Analogue-Conjugated BN Nanomaterials in a Solvated Phase: First Principles Study of Topology-Dependent Interactions with a Monolayer and a (5,0) Nanotube

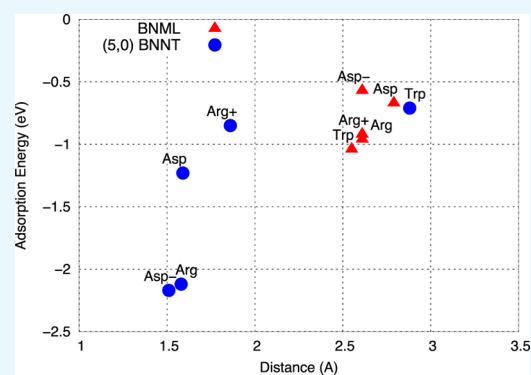
Kevin Waters,^{*,†} Ravindra Pandey,^{*,†} and Shashi P. Karna[‡]

[†]Department of Physics, Michigan Technological University, Houghton, Michigan 49931, United States

[‡]Weapons and Materials Research Directorate, U.S. Army Research Laboratory, ATTN: RDRL-WM, Aberdeen Proving Ground, Aberdeen, Maryland 21005-5069, United States

S Supporting Information

ABSTRACT: Using density functional theory and an implicit solvation model, the relationship between the topology of boron nitride (BN) nanomaterials and the protonated/deprotonated states of amino acid analogues is investigated. In the solvated phase, the calculated results show distinct “physisorbed versus chemisorbed” conditions for the analogues of arginine (Arg)- and aspartic acid (Asp)-conjugated BN nanomaterials, including a monolayer (ML) and a small-diameter zigzag nanotube (NT). Such a distinction does not depend on the functional groups of amino acids but rather depends on the curvature-induced interactions associated with the tubular configuration. Arg and Asp interact with the BNML to form physisorbed complexes irrespective of the state of the amino acids in the solvated phase. For the NT, Arg and Asp form chemisorbed complexes, and the distinct nature of bonds between the donor electron moieties of N_(Arg) and O_(Asp) and the boron of the tubular surface is revealed by the natural bond orbital analysis; stronger s-type bonds for the deprotonated conjugated complexes and slightly weaker p-type dominated bonds for the protonated conjugated complexes. The interaction of neutral Trp with BN nanomaterials results in physisorbed configurations through π -stacking interactions with the indole ring of the Trp and BN nanomaterials. The calculated results form the basis for a theoretical study of more complex protein macromolecules interacting with nanomaterials under physiological conditions.



1. INTRODUCTION

Nanomaterials with different topologies possess unique and distinct properties that can be exploited for biologically related applications, such as biosensing,¹ drug delivery,² and bioimaging.³ Some of the topologies that have been investigated as substrates for these applications include nanotubes (NTs),^{1,4} nanowires,⁵ nanoparticles,⁶ nanorods,⁷ and two-dimensional (2D) sheets.⁸ Boron nitride NTs⁹ (BNNTs), one of the emerging nanomaterials, have a morphology similar to that of the well-established carbon NTs (CNTs). BNNTs are recognized as viable candidates for conjugation with biomolecules,¹⁰ showing a strong affinity toward proteins.¹¹ However, experiments show contrasting results in terms of the toxicity effects of BNNTs.¹²

To provide a strong foundation for the biologically related applications of BN nanomaterials, the nature of the interface has been the focus of several theoretical investigations. For DNA and RNA nucleotides, physisorbed configurations were predicted.¹³ For amino acids interacting with BNNTs, the calculated results show that arginine (Arg) and aspartic acid (Asp) exhibit relatively strong bonds with the surface of the BNNTs relative to the case of tryptophan (Trp).¹⁴ A recent

theoretical study considering only the side chains of α -amino acids interacting with a (6,0) BNNT and a BN monolayer (ML) reported that the nature of the interaction strongly depends on the side chain of the analogue molecules in the gas phase.^{14b} Interactions of the neutral configurations of the basic and acidic amino acids with both the ML and NT appeared to be weak and associated with the oxygen-containing side groups (e.g., serine, Asp, glutamic acid, asparagine, and glutamine). Stronger interactions with the BNNTs are predicted by the presence of nitrogen-containing groups (e.g., lysine, histidine, and Arg). The aromatic amino acids (e.g., Trp, tyrosine, and phenylalanine) weakly interact with the BNNTs. For the case of BNML, dispersive-type interactions follow the order of aromatic > N-containing groups > O-containing groups of amino acid analogues in the gas phase.

As physiological conditions include the presence of water, theoretical results obtained for the gas phase may not provide a direct correlation to experimental results. This is due to the

Received: October 19, 2016

Accepted: December 29, 2016

Published: January 9, 2017

Table 1. Amino Acid-Conjugated BN Nanomaterials in the Solvated Phase: Adsorption Energy, Nearest-Neighbor Distance, Mulliken Charge Transfer (ΔQ), and Dipole Moment Obtained Using the Polarizable Continuum Model (PCM) at the DFT (PBE-D2) Level of Theory^a

amino acids	$E_{\text{adsorption}}$ (eV)	nearest-neighbor distance	R (Å)	ΔQ (e)	dipole moment (D)
BNML					
charged					
Arg (+) (protonated)	-0.92	$R(\text{N}_{\text{ML}}-\text{H})$	2.61	-0.1	15.0
Asp (-) (deprotonated)	-0.57	$R(\text{B}_{\text{ML}}-\text{H})$	2.61	+0.1	11.6
neutral					
Arg (deprotonated)	-0.96	$R(\text{B}_{\text{ML}}-\text{H})$	2.61	≈ 0.0	5.9
Asp (protonated)	-0.67	$R(\text{N}_{\text{ML}}-\text{H})$	2.79	≈ 0.0	7.4
Trp	-1.04	$R(\text{B}_{\text{ML}}-\text{H})$	2.55	≈ 0.0	1.2
(5,0) BNNT					
charged					
Arg (+) (protonated)	-0.85	$R(\text{B}_{\text{NT}}-\text{N})$	1.86	+0.1	27.9
Asp (-) (deprotonated)	-2.17	$R(\text{B}_{\text{NT}}-\text{O})$	1.51	+0.6	13.4
neutral					
Arg (deprotonated)	-2.12	$R(\text{B}_{\text{NT}}-\text{N})$	1.58	+0.4	14.8
Asp (protonated)	-1.23	$R(\text{B}_{\text{NT}}-\text{O})$	1.59	+0.3	12.8
Trp	-0.71	$R(\text{N}_{\text{NT}}-\text{H})$	2.88	+0.1	7.3

^aNegative ΔQ represents charge transfer from BNML (BNNT) to molecule. In the solvated phase, the protonated Arg and deprotonated Asp have charges of +1 and -1, respectively.

occurrence of different protonated states within the amino acids in the solvated phase. This is addressed in this study by considering the interaction of the analogues of Arg, Asp, and Trp with a BNML and a (5,0) zigzag-type BNNT in a solvated phase. It is important to note that a small-diameter BNNT was chosen for its large curvature and BNML was chosen for the lack of curvature, facilitating the end points to examine the role of topology in defining the interface of the conjugated complexes in the solvated phase. Armchair and zigzag BNNTs may show different characteristics, with the latter found to be more reactive, thereby providing an end point for the investigation.¹⁵ The role of curvature can be expressed in terms of induced strain of the sp^2 bonds in defining the nature of the interface for the conjugated BN nanomaterials. The smaller zigzag NTs have greater strain as compared to that of the armchair configurations.¹⁶ Both zigzag and armchair NTs converge to the same properties exhibited by larger NTs;¹⁷ for this reason, armchair NTs were not considered in this study.

The amino acids considered are Arg and Asp, representing basic and acidic side-chain functional groups, respectively, and Trp for its aromatic properties. Asp is a polar amino acid with a side chain of carboxylic that can be protonated/deprotonated, resulting in a net neutral/negative charge, and Arg is a polar amino acid with a side chain of guanidyl that can be protonated/deprotonated, resulting in a net positive/neutral charge. Under the physiological condition of pH 7, both the amino acids are charged, with Arg being protonated and Asp being deprotonated. The equilibrium configurations of the conjugated complexes were analyzed in terms of binding energy, bond distances, and Mulliken charges to gain insight into the nature of the interface under solvated conditions. Specifically, the calculated results are expected to shed light on the topological and chemical conditions for “physisorption versus chemisorption” of amino acids interacting with BN nanomaterials under physiological conditions.

2. RESULTS AND DISCUSSION

To benchmark the calculated results, we first report the gas-phase results of Trp-, Arg-, and Asp-conjugated BN nanoma-

terials. Later, results of the solvated-phase calculations considering the different protonated states of Arg and Asp interacting with BN nanomaterials are presented.

In gas phase, the calculated results are in qualitative agreement (Table S1 of the Supporting Information) with those obtained using the periodic supercell models.^{14b,d} The effect of the inclusion of dispersive interaction correction term D2 on the calculated energies (Table S2) was also investigated. For all cases, the D2 term shows its importance in capturing contributions from dispersive interactions, which are generally dominant in the conjugated complexes considered.

It is known that the interaction of Trp with nanomaterials is governed by long-range dispersive interactions, with a capability of forming weak ionic bonds in a conjugated system. Calculations at the density functional theory (DFT) (Perdew, Becke, and Ernzerhof (PBE)) level of theory find the adsorption energy to be +0.02 eV for Trp-conjugated BNML. Inclusion of the D2 term yields the value of -0.74 eV for BNML. This is not the case with Trp-conjugated BNNT, where the increase in adsorption energy is small after including the D2 term. The calculated adsorption energies are -0.74 and -0.29 eV for BNML and BNNT, respectively, at the DFT (PBE-D2) level of theory. The reduced surface area of the BNNT decreases the interaction with Trp relative to that available for BNML. This is what has also been seen for the cases of organic molecules interacting with the BN nanomaterials in the gas phase.^{13b,14c,18}

Inclusion of the basis set superposition error (BSSE) correction term lowers the adsorption energy while maintaining the hierarchy of the interaction strength: protonated Asp < deprotonated Arg < Trp < deprotonated Asp < protonated Arg toward BNML and Trp < protonated Asp < protonated Arg < deprotonated Arg < deprotonated Asp toward BNNT (Table S2). The calculations involving the interaction of BNML with amino acids were performed with the ML frozen; relaxing the ML configuration only slightly lowered the adsorption energy. The calculated difference in the adsorption energy of Asp interacting with the frozen and relaxed MLs was about 0.01 eV at the DFT (PBE-D2) level of theory. The results for the

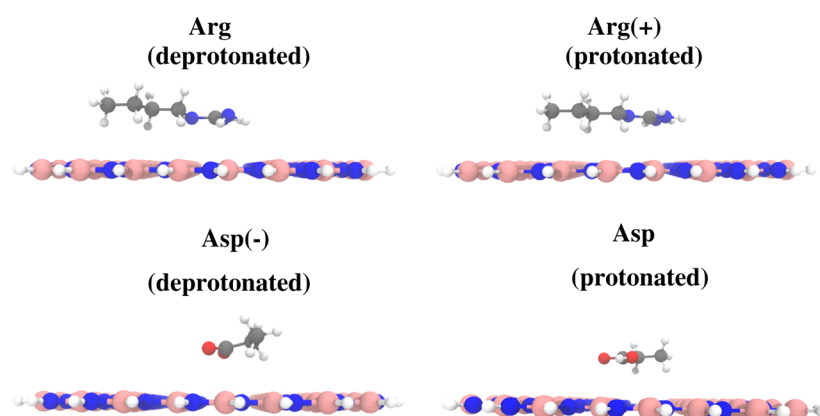


Figure 1. Calculated equilibrium configurations of Arg- and Asp-conjugated BNML (atomic symbols: N (blue), B (pink), C (black), and H (white)).

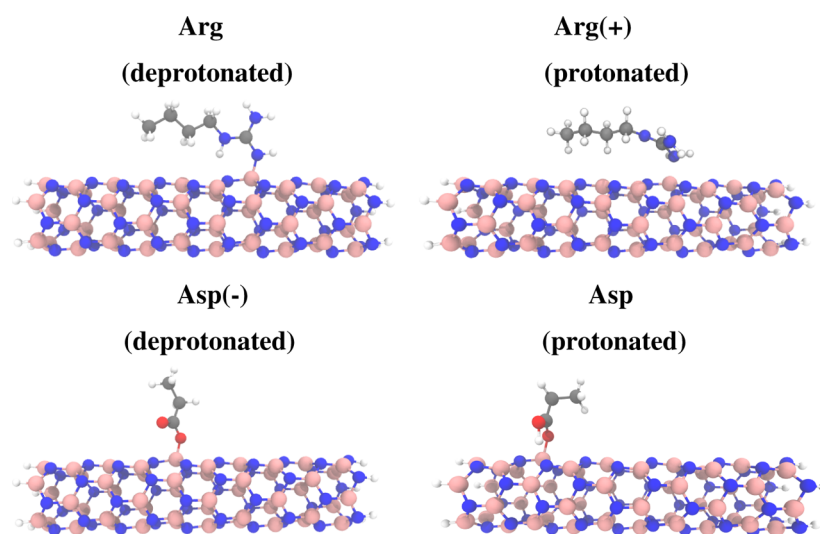


Figure 2. Calculated equilibrium configurations of Arg- and Asp-conjugated BNNT (atomic symbols: N (blue), B (pink), C (black), and H (white)).

tubular configurations were obtained by constraint-free optimization of BNNT interacting with amino acids.

In the solvated phase, the calculated adsorption energies of Arg, Asp, and Trp interacting with the BNML and the (5,0) BNNT obtained at the DFT (PBE-D2) level of theory are listed in Table 1. The calculated nearest-neighbor distances between the amino acids and BN nanomaterials, Mulliken charge transfer, and dipole moments associated with the equilibrium configurations are also given in Table 1. The calculated equilibrium configurations of amino acids interacting with BNML and BNNT are displayed in Figures 1, 2, and S1.

When conjugated with the BNML, the interactions are dominated by the long-range dispersive interactions, yielding physisorbed configurations (Figure 1). This is affirmed by the noticeable increase in the adsorption energies after the inclusion of the D2 correction term in calculations; the BNML-conjugated complexes show an order of magnitude increase in the adsorption energies relative to that of the BNNT-conjugated complexes (Table S2). In the solvated phase, the protonated or deprotonated Arg and Asp interacting with BN nanomaterials have similar adsorption energies (−0.57 to −0.96 eV) and near-neighbor distances (2.61–2.79 Å). A negligible charge transfer occurs in BNML complexes, and the charged BNML complexes have a higher dipole moment relative to that of neutral BNML complexes as expected.

For BNNT, the calculated results show a difference between the chemisorbed configurations of the protonated and deprotonated complexes (Figures 2). The protonated Arg (i.e., Arg(+)) forms a bond between N (amino group) and B (tubular surface) atoms, with the near-neighbor distance and adsorption energy of 1.86 Å and −0.85 eV, respectively. Mulliken charge analysis shows a small charge transfer between Arg(+) and BNNT. The protonated Asp prefers to interact with the O (carboxyl group) in the equilibrium configuration, with the near-neighbor distance and adsorption energy of 1.59 Å and −1.23 eV, respectively; a larger charge transfer from the BNNT to Asp also accompanies it. The increased electronegativity of oxygen in Asp yields a stronger interaction of the protonated Asp with BNNT.

The interaction energies and distances are summarized in Figure 3. The deprotonated Arg and Asp interact with the BNNT to form stable complexes, where Asp and Arg are chemisorbed on the NT surface with a higher adsorption energy of about −2.1 eV and a smaller near-neighbor distance of 1.5–1.6 Å. The nearest-neighbor distance of Arg-conjugated BNNT (i.e., $R_{\text{BNNT-N}}$) is similar to that of the cubic BN,¹⁹ suggesting a sp^3 -type bond at the tubular surface. A higher charge transfer from BN nanomaterials to the deprotonated Arg and Asp suggests the interaction to be partially ionic in the conjugated complexes. It should be noted that the deprotonated Arg and Asp exist together only at a basic pH. The low

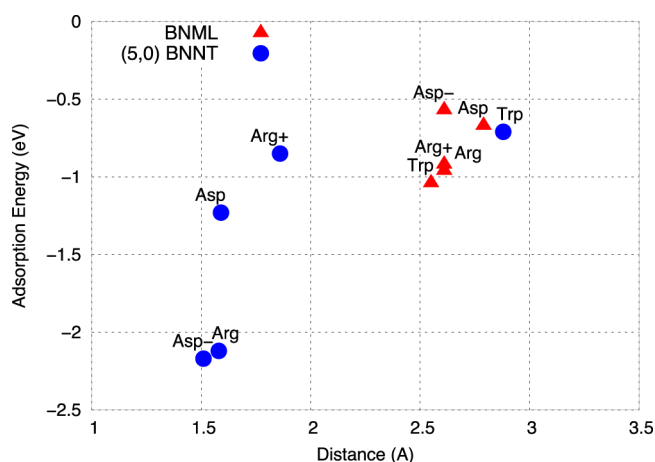


Figure 3. Physisorbed vs chemisorbed configurations in the solvated phase: adsorption energy vs near-neighbor distance of amino acid-conjugated BN complexes.

pK_a value (3.86) of Asp does not facilitate its coexistence with Arg at a neutral pH.

To ascertain the nature of bonding in chemisorbed configurations, natural bond orbital (NBO) analysis is performed for the BNNT complexes. For deprotonated amino acids, B_{BNNT} atom on the tubular surface changes its local environment; originally, its characteristic is a strained $sp^{1.9-2.2}$ bond. When conjugated, the B atom accommodates the newly formed bonds with the neighboring N_{BNNT} atoms. The bond characteristics are $sp^{2.83}$ ($sp^{2.71}$), $sp^{2.92}$ ($sp^{3.02}$), and $sp^{2.86}$ ($sp^{2.71}$) for the deprotonated Arg (Asp^-)-conjugated complexes, whereas the bond characteristic of the $B_{\text{BNNT}}-N_{\text{AA}}$ (O_{AA}) bond is predicted to be $sp^{3.42}$ ($sp^{3.66}$) for the deprotonated Arg (Asp^-)-conjugated complexes. The tubular surface atoms, therefore, form sp^3 -like bonds in the deprotonated complexes. Interestingly, the protonated amino acids show sp^2 -like characteristics with a larger p -orbital contribution from B_{BNNT} atom in the conjugated complexes. The B_{BNNT} bonds are predicted to have characteristics of $sp^{2.28}$ ($sp^{2.56}$), $sp^{2.41}$ ($sp^{2.57}$), and $sp^{2.43}$ ($sp^{2.63}$) for Arg^+ (Asp)-conjugated complexes. The bond characteristic of the $B_{\text{BNNT}}-N_{\text{AA}}$ (O_{AA}) bond is $sp^{7.99}$ ($sp^{5.06}$) for the Arg^+ (Asp) complexes.

The calculated adsorption energies are in a stark contrast with the results of a recent DFT (B3LYP-D2) study²⁰ employing a finite cluster model. For the cases of Arg and Asp interacting with BNML, the reported energy values²⁰ are -172.21 kcal/mol (-7.46 eV) and -156.96 kcal/mol (-6.81 eV), respectively. These values seem inconsistent as they are significantly higher relative to the PBE-D2 results together with

the results of the periodic supercell model employing the B3LYP-D2 functional form.^{14b}

Considering that Trp is a nonpolar aromatic amino acid, investigation of an interaction of Trp with BN nanomaterials in the solvated phase can quantify the effect of solvated phase with reference to gas-phase results. In the solvated phase, Trp stabilizes in the physisorbed configurations with π -stacking interactions with the indole ring of Trp and BN nanomaterials, as was the case in the gas phase (Figure S2). The calculated results agree with recent experimental results, suggesting physisorption of Trp on BNML.²¹

In the solvated phase, the calculated results show that the interaction strength with BNML follows the order of deprotonated Arg > protonated Arg(+) > protonated Asp > deprotonated Asp(-). This is slightly different for BNNT, with the hierarchy being deprotonated Asp(-) > deprotonated Arg > protonated Asp > protonated Arg(+). The interaction strength in terms of the adsorption energy shows a contrasting behavior for BNML and BNNT complexes; BNMLs prefer to form physisorbed complexes irrespective of the charge states of amino acids, and BNNTs prefer to form chemisorbed complexes via the formation of a covalent bond dictated by either dominant p -type (e.g., protonated Arg) or s -type (e.g., deprotonated Asp) electronic states.

We are aware of the fact that the PCM may not accurately represent the interaction of amino acids with water molecules. In general, the presence of H-bond networks between the amino acid-conjugated complexes in the solvated phase is likely to modify the equilibrium geometries. This fact was examined for the case of deprotonated Arg interacting with both the BNML and BNNT using explicit solvation by including six water molecules. The calculated results shown in Figure 4 reflect the configurations obtained using the implicit solvation model. The conclusion is that the topological variation determines the physisorbed versus chemisorbed state for amino acids interacting with BN nanomaterials. Furthermore, it is found that water molecules do not dominate the interface between the amino acids and the BN nanomaterials. Interestingly, both theoretical and experimental studies revealed the hydrophobic nature of pristine BNNT.^{14b,22}

It should be noted here that capturing of the physics and chemistry of the solvation effect by the PCM was demonstrated in a theoretical study of the zwitterionic forms of glycine and alanine.²³ Our recent study of the interaction of DNA with chalcogenide quantum dots also shows an effective screening of the electrostatic interaction between QD and DNA by the solvation model.²⁴ Considering that Figure 4 represents the results of limited DFT calculations, we plan to use the molecular dynamics method to obtain a detailed atomistic view

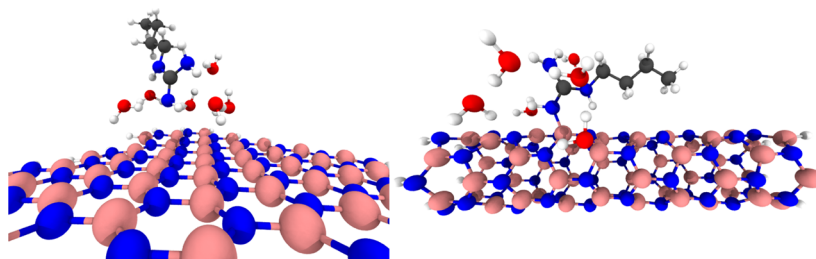


Figure 4. Deprotonated Arg interacting with BNML (left) and (5,0) BNNT (right) in the presence of several water molecules (atoms: H (white), B (pink), C (gray), N (blue), and O (red)).

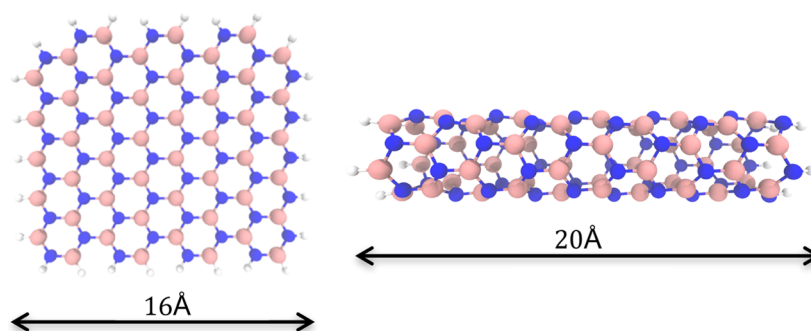


Figure 5. Cluster models of BN nanomaterials: (left) BNML represented by the $(B_{49}N_{49}H_{22})$ cluster and (right) (5,0) BNNT represented by the $(B_{50}N_{50}H_{10})$ cluster. The cluster edge atoms are passivated with H atoms (atomic symbols: N (blue), B (pink), and H (white)).

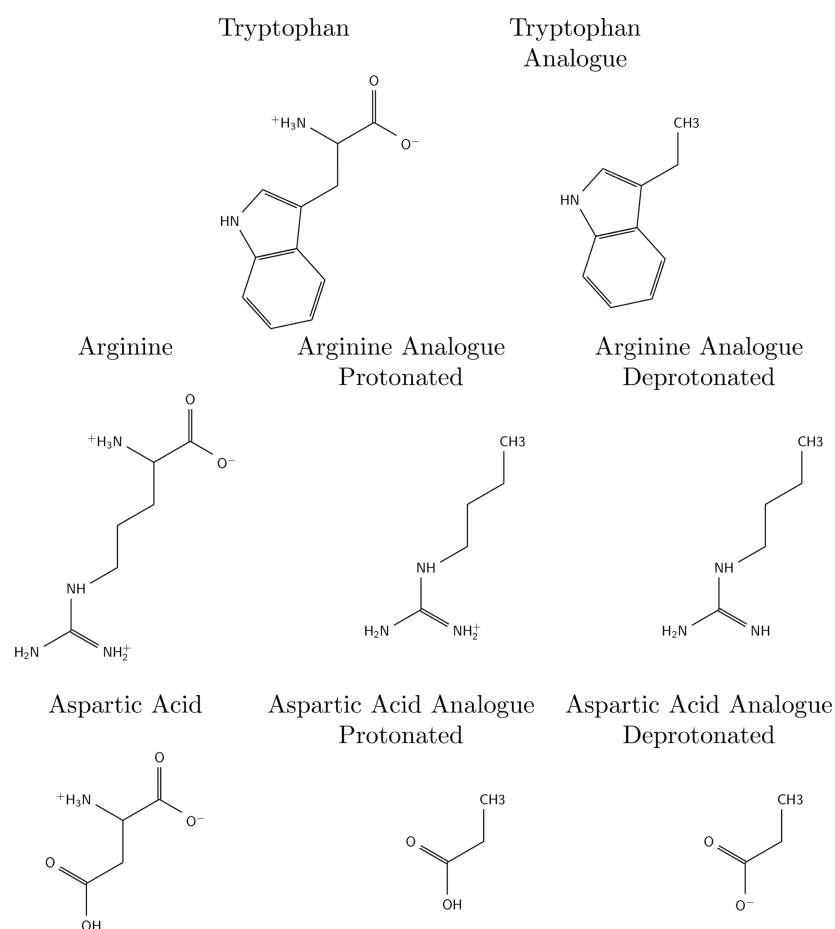


Figure 6. Chemical structures of the amino acids considered. The first column is the amino acid in its zwitterionic form, followed by the analogues in different protonated states. In the analogues, the backbone is replaced by a $-CH_3$ group.

of the interface of amino acid-conjugated BN nanomaterials in the solvated phase.

3. COMPUTATIONAL MODEL

The BNML and BNNT configurations were represented by finite cluster models, as shown in Figure 5. The BNML ($18 \text{ \AA} \times 16 \text{ \AA}$) was simulated using a $B_{49}N_{49}H_{22}$ cluster, and the (5,0) BNNT ($4 \text{ \AA} \times 20 \text{ \AA}$) was simulated using a $B_{50}N_{50}H_{10}$ cluster. The cluster edge atoms were passivated by hydrogen atoms to ensure their appropriate coordination in both the ML and tubular configurations.²⁵ The cluster model has been successfully used to describe the properties and interactions

that are localized in nature,²⁶ such as the cases considered in the present study.

The DFT calculations were carried out using the Gaussian09 program package.²⁷ The exchange and correlation functional form was represented by the PBE functional form.²⁸ The 6-31g(d,p) basis set²⁹ was used for the constituent atoms of the amino acids and BN nanomaterials. Grimme's D2 semi-empirical approximation was included within DFT via a posteriori term to the total energy of the system.³⁰ The importance of the inclusion of the dispersive term has been emphasized in previous calculations of interfaces consisting of BN nanomaterials.^{14a-c,20}

Initially, constraint-free geometry optimizations of the complexes were performed to determine the preferred orientation and optimum height of amino acid relative to the surface of nanomaterial with the exception of BNML, where sheet was frozen to mimic its periodic nature. This step was then followed by further calculations, including (i) height scan of the molecule perpendicular to the surface in incremental steps of 0.1 Å and (ii) surface grid scan in steps of 0.25 Å at the height obtained in step (i). A representative energy surface obtained by scanning a 4 Å × 4 Å area with 400 grid points is shown in Figure S2. These calculations were performed at each level of theory, including PBE (gas phase), PBE-D2 (gas phase), and PBE-D2 (solvated). It is worth noting that a similar procedure has been successfully employed to obtain the equilibrium configurations of the complexes consisting of organic molecules interacting with graphene, CNT, and BNNTs.^{14d,31}

To test the reliability of the cluster model, a comparison is made with the properties calculated using the periodic supercell model^{14c} (Table S1). For BNNT, the bond lengths (R_{BN}) along the tube axis and the zigzag direction are 1.45 and 1.47 Å, respectively; periodic DFT calculations also showed the same values of R_{BN} .^{14c} For BNML, the calculated R_{BN} is 1.45 Å, which is in agreement with the previously reported value of 1.45 Å.^{14c} The semi-ionic nature of bonding displayed in the cluster model is similar to that predicted by the periodic model, with N having negative charge in the 2D lattice.²⁵ Both the ML and tubular configurations are predicted to be semiconducting.^{14c} For the ML, the calculated energy gap between the highest occupied molecular orbital (HOMO) and the lowest unoccupied molecular orbital (LUMO) is 4.1 eV, which compares well with the previously reported value of 4.6 eV obtained using DFT (B3LYP).^{14c} The calculated HOMO–LUMO gap in (5,0) BNNT is 1.7 eV at the DFT (PBE) level of theory. BNNTs show band gap properties similar to those of their analogue CNT for tubes smaller than (15,0) or (15,15).³² In general, the inner electronic states interact with tubes having smaller diameter, thereby reducing the band gap, as was calculated for zigzag-type ($n,0$) BNNTs.¹⁷

The α -amino acids contain amine ($-\text{NH}_2$) and carboxylic acid ($-\text{COOH}$) groups, which are connected with the α -C, forming the backbone of amino acids. Each amino acid is characterized by its side chain attached to the α -C. The side chains range from one hydrogen atom to an indole group, giving each a unique functionality. The backbones form polypeptide chains, which then fold to form a complex protein structure. In a recent calculation, a methyl group (CH_3) is used to represent a termination of the backbone, mimicking the protein configuration in a computationally efficient way.^{14b} Amino acid analogues are then defined as $[\text{CH}_3\text{-R}]$ molecules consisting of the side chain (R) and the α -C terminated by three H atoms (Figure 6). This approximation is similar to the one employed previously with the exception that the α -C atom is also excluded from the configurations.^{14b,33}

Each amino acid has specific pK_a (i.e., logarithmic acid dissociation constant) values for the dissociation of each proton. The pK_a of the Asp side chain is 3.65, indicating that the side chain can be protonated or deprotonated. The calculated results find small differences between the protonated and deprotonated structures at the PBE-D2 level of theory (e.g., $R_{\text{O-C}}$ is 1.21 (1.26) Å and the $R_{\text{C-C}}$ is 1.53 (1.59) Å in the protonated (deprotonated) Asp). This is also the case with Arg,

where $R_{\text{NH}_2\text{-C}}$ is 1.35 (1.40) Å and the $R_{\text{C-N}}$ is 1.33 (1.40) Å in the protonated (deprotonated) Arg.

As biological processes occur in a solvated environment, inclusion of the effect of such environment in a theoretical model is necessary for accurate calculations. This fact has also been brought out by calculations on glycine-conjugated BNNT.^{14a} In this study, the implicit solvation was modeled using a PCM.³⁴ This model simulates the solvent by representing it as a homogenous continuum medium with a dielectric constant of 78.36 (for water). The adsorption energy of amino acids interacting with the BN nanomaterials is then calculated using the following equation

$$E_{\text{adsorption}} = E_{\text{complex}} - (E_{\text{nanomaterial}} + E_{\text{molecule}}) - E_{\text{BSSE}} \quad (1)$$

where E_{complex} is the total energy of a bioconjugated complex, $E_{\text{nanomaterial}}$ is the total energy of BNML or BNNT, E_{molecule} is the total energy of the amino acids considered, and E_{BSSE} is the BSSE, which was calculated using the counterpoise method.³⁵ The BSSE can only be calculated for the gas phase. NBO analysis was also conducted on the conjugated NT to characterize the nature of bonding of the chemisorbed states in the conjugated BNNT complexes.³⁶

4. SUMMARY

The interactions of neutral and charged amino acid analogues with BN nanomaterials are investigated in a solvated environment using the implicit solvation model. The calculated results based on DFT show that the deprotonated states of the polar amino acids facilitate the formation of chemically bound states between the donor electron moieties (i.e., $\text{O}_{(\text{Asp})}$ and $\text{N}_{(\text{Arg})}$) and the NT surface of B_{BNNT} . In the absence of curvature for the BNML, the amino acids form physisorbed complexes, which are governed by dispersive interactions. The calculated results show that BNNTs would have the ability to immobilize proteins through strong interactions with the acidic and basic amino acids and therefore can be used in health-related applications.

■ ASSOCIATED CONTENT

Supporting Information

The Supporting Information is available free of charge on the ACS Publications website at DOI: 10.1021/acsomega.6b00321.

Calculated equilibrium configurations together with the effects of dispersion corrections and BSSE terms on the calculated adsorption energies (PDF)

■ AUTHOR INFORMATION

Corresponding Authors

*E-mail: kwaters@mtu.edu (K.W.).

*E-mail: pandey@mtu.edu. Phone: 906-487-2086 (R.P.).

ORCID

Kevin Waters: 0000-0003-3828-8647

Notes

The authors declare no competing financial interest.

■ ACKNOWLEDGMENTS

Helpful discussions with Nabanita Saikia, Max Seel, Wil Slough, and Gaoxue Wang are acknowledged. RAMA and Superior, high-performance computing clusters at Michigan Technological University, were used to obtain the results presented in this

article. This research was partially supported by the Army Research Office through grant number W911NF-14-2-0088.

REFERENCES

- (1) Chen, R. J.; Bangsaruntip, S.; Drouvalakis, Ka; Kam, N. W. S.; Shim, M.; Li, Y.; Kim, W.; Utz, P. J.; Dai, H. Noncovalent functionalization of carbon nanotubes for highly specific electronic biosensors. *Proc. Natl. Acad. Sci. U.S.A.* **2003**, *100*, 4984–4989.
- (2) Saikia, N.; Deka, R. C. Density functional study on noncovalent functionalization of pyrazinamide chemotherapeutic with graphene and its prototypes. *New J. Chem.* **2014**, *38*, 1116.
- (3) Li, J.; Zhu, J. J. Quantum dots for fluorescent biosensing and bioimaging applications. *Analyst* **2013**, *138*, 2506–15.
- (4) (a) Chen, R. J.; Zhang, Y.; Wang, D.; Dai, H. Noncovalent side-wall functionalization of single-walled carbon nanotubes. *J. Am. Chem. Soc.* **2001**, *123*, 3838–3839. (b) Kang, Y.; Liu, Y. C.; Wang, Q.; Shen, J. W.; Wu, T.; Guan, W. J. On the spontaneous encapsulation of proteins in carbon nanotubes. *Biomaterials* **2009**, *30*, 2807–15. (c) Pantarotto, D.; Partidos, C. D.; Graff, R.; Hoebeke, J.; Briand, J. P.; Prato, M.; Bianco, A. Synthesis, Structural Characterization, and Immunological Properties of Carbon Nanotubes Functionalized with Peptides. *J. Am. Chem. Soc.* **2003**, *125*, 6160–6164. (d) Wong, S. S.; Joselevich, E.; Woolley, A. T.; Cheung, C. L.; Lieber, C. M. Covalently functionalized nanotubes as nanometre-sized probes in chemistry and biology. *Nature* **1998**, *394*, 52–55.
- (5) Cui, Y.; Wei, Q.; Park, H.; Lieber, C. M. Nanowire nanosensors for highly sensitive and selective detection of biological and chemical species. *Science* **2001**, *293*, 1289–1292.
- (6) Hong, R.; Fischer, N. O.; Verma, A.; Goodman, C. M.; Emrick, T.; Rotello, V. M. Control of Protein Structure and Function through Surface Recognition by Tailored Nanoparticle Scaffolds. *J. Am. Chem. Soc.* **2004**, *126*, 739–743.
- (7) Cao, J.; Sun, T.; Grattan, K. T. V. Gold nanorod-based localized surface plasmon resonance biosensors: A review. *Sens. Actuators, B* **2014**, *195*, 332–351.
- (8) Singh, A.; Sinsinbar, G.; Choudhary, M.; Kumar, V.; Pasricha, R.; Verma, H. N.; Singh, S. P.; Arora, K. Graphene oxide-chitosan nanocomposite based electrochemical DNA biosensor for detection of typhoid. *Sens. Actuators, B* **2013**, *185*, 675–684.
- (9) Chopra, N. G.; Luyken, R. J.; Cherrey, K.; Crespi, V. H.; Cohen, M. L.; Louie, S. G.; Zettl, A. Boron nitride nanotubes. *Science* **1995**, *269*, 966–967.
- (10) Golberg, D.; Bando, Y.; Huang, Y.; Terao, T.; et al. Boron nitride nanotubes and nanosheets. *ACS Nano* **2010**, *4*, 2979–2993.
- (11) Zhi, C.; Bando, Y.; Tang, C.; Golberg, D. Immobilization of proteins on boron nitride nanotubes. *J. Am. Chem. Soc.* **2005**, *127*, 17144–17145.
- (12) (a) Del Turco, S.; Ciofani, G.; Cappello, V.; Gemmi, M.; Cervelli, T.; Saponaro, C.; Nitti, S.; Mazzolai, B.; Basta, G.; Mattoli, V. Cytocompatibility evaluation of glycol-chitosan coated boron nitride nanotubes in human endothelial cells. *Colloids Surf., B* **2013**, *111*, 142–9. (b) Fernandez-Yague, M. A.; Larranaga, A.; Gladkovskaya, O.; Stanley, A.; Tadayyon, G.; Guo, Y.; Sarasua, J. R.; Tofail, S. A.; Zeugolis, D. I.; Pandit, A.; Biggs, M. J. Effects of Polydopamine Functionalization on Boron Nitride Nanotube Dispersion and Cytocompatibility. *Bioconjugate Chem.* **2015**, *26*, 2025–37. (c) Ferreira, T. H.; Soares, D. C. F.; Moreira, L. M. C.; da Silva, P. R. O.; dos Santos, R. G.; de Sousa, E. M. B. Boron nitride nanotubes coated with organic hydrophilic agents: Stability and cytocompatibility studies. *Mater. Sci. Eng., C* **2013**, *33*, 4616–4623. (d) Yang, C.-K. Exploring the interaction between the boron nitride nanotube and biological molecules. *Comput. Phys. Commun.* **2011**, *182*, 39–42.
- (13) (a) Zhong, X.; Mukhopadhyay, S.; Gowtham, S.; Pandey, R.; Karna, S. P. Applicability of carbon and boron nitride nanotubes as biosensors: Effect of biomolecular adsorption on the transport properties of carbon and boron nitride nanotubes. *Appl. Phys. Lett.* **2013**, *102*, No. 133705. (b) Mukhopadhyay, S.; Gowtham, S.; Scheicher, R. H.; Pandey, R.; Karna, S. P. Theoretical study of physisorption of nucleobases on boron nitride nanotubes: a new class of hybrid nano-biomaterials. *Nanotechnology* **2010**, *21*, No. 165703.
- (14) (a) Rimola, A.; Sodupe, M. Gas-Phase and Microsolvated Glycine Interacting with Boron Nitride Nanotubes. A B3LYP-D2* Periodic Study. *Inorganics* **2014**, *2*, 334–350. (b) Rimola, A. Intrinsic Ladders of Affinity for Amino-Acid-Analogues on Boron Nitride Nanomaterials: A B3LYP-D2* Periodic Study. *J. Phys. Chem. C* **2015**, *119*, 17707–17717. (c) Rimola, A.; Sodupe, M. Physisorption vs. chemisorption of probe molecules on boron nitride nanomaterials: the effect of surface curvature. *Phys. Chem. Chem. Phys.* **2013**, *15*, 13190–8. (d) Mukhopadhyay, S.; Scheicher, R. H.; Pandey, R.; Karna, S. P. Sensitivity of Boron Nitride Nanotubes toward Biomolecules of Different Polarities. *J. Phys. Chem. Lett.* **2011**, *2*, 2442–2447.
- (15) (a) Kaur, J.; Singla, P.; Goel, N. Adsorption of oxazole and isoxazole on BNNT surface: A DFT study. *Appl. Surf. Sci.* **2015**, *328*, 632–640. (b) Chermahini, A. N.; Teimouri, A.; Farrokhpour, H. Theoretical studies of urea adsorption on single wall boron-nitride nanotubes. *Appl. Surf. Sci.* **2014**, *320*, 231–236.
- (16) Blase, X.; Rubio, A.; Louie, S. G.; Cohen, M. L. Stability and Band Gap Constancy of Boron Nitride Nanotubes. *Europhys. Lett.* **1994**, *28*, 335–340.
- (17) Zhang, Z.; Guo, W.; Dai, Y. Stability and electronic properties of small boron nitride nanotubes. *J. Appl. Phys.* **2009**, *105*, No. 084312.
- (18) Akdim, B.; Kim, S. N.; Naik, R. R.; Maruyama, B.; Pender, M. J.; Pachter, R. Understanding effects of molecular adsorption at a single-wall boron nitride nanotube interface from density functional theory calculations. *Nanotechnology* **2009**, *20*, No. 355705.
- (19) Petrescu, M. I.; Balint, M. Structure and properties modification in boron nitride. Part I: Direct polymorphic transformations mechanisms. *Sci. Bull. - Univ. "Politeh." Bucharest, Ser. B* **2007**, *69*, 35–42.
- (20) Singla, P.; Riyaz, M.; Singhal, S.; Goel, N. Theoretical study of adsorption of amino acids on graphene and BN sheet in gas and aqueous phase with empirical DFT dispersion correction. *Phys. Chem. Chem. Phys.* **2016**, *18*, 5597–604.
- (21) Mallineni, S. S. K.; Shannahan, J.; Raghavendra, A. J.; Rao, A. M.; Brown, J. M.; Podila, R. Biomolecular Interactions and Biological Responses of Emerging Two-Dimensional Materials and Aromatic Amino Acid Complexes. *ACS Appl. Mater. Interfaces* **2016**, *8*, 16604–16611.
- (22) Li, L.; Li, L. H.; Ramakrishnan, S.; Dai, X. J.; Nicholas, K.; Chen, Y.; Chen, Z.; Liu, X. Controlling Wettability of Boron Nitride Nanotube Films and Improved Cell Proliferation. *J. Phys. Chem. C* **2012**, *116*, 18334–18339.
- (23) Chowdhry, B. Z.; Dines, T. J.; Jabeen, S.; Withnall, R. Vibrational Spectra of α -Amino Acids in the Zwitterionic State in Aqueous Solution and the Solid State: DFT Calculations and the Influence of Hydrogen Bonding. *J. Phys. Chem. A* **2008**, *112*, 10333–10347.
- (24) Wang, Z.; He, H.; Slough, W.; Pandey, R.; Karna, S. P. Nature of Interaction between Semiconducting Nanostructures and Biomolecules: Chalcogenide QDs and BNNT with DNA Molecules. *J. Phys. Chem. C* **2015**, *119*, 25965–25973.
- (25) Seel, M.; Pandey, R. Proton and hydrogen transport through two-dimensional monolayers. *2D Mater.* **2016**, *3*, No. 025004.
- (26) Saikia, N.; Seel, M.; Pandey, R. Stability and Electronic Properties of 2D Nanomaterials Conjugated with Pyrazinamide Chemotherapeutic: A First-Principles Cluster Study. *J. Phys. Chem. C* **2016**, *120*, 20323–20332.
- (27) Frisch, M. J.; Trucks, G. W.; Schlegel, H. B.; Scuseria, G. E.; Robb, M. A.; Cheeseman, J. R.; Scalmani, G.; Barone, V.; Mennucci, B.; Petersson, G. A.; Nakatsuji, H.; Caricato, M.; Li, X.; Hratchian, H. P.; Izmaylov, A. F.; Bloino, J.; Zheng, G.; Sonnenberg, J. L.; Hada, M.; Ehara, M.; Toyota, K.; Fukuda, R.; Hasegawa, J.; Ishida, M.; Nakajima, T.; Honda, Y.; Kitao, O.; Nakai, H.; Vreven, T.; Montgomery, J. A., Jr.; Peralta, J. E.; Ogliaro, F.; Bearpark, M.; Heyd, J. J.; Brothers, E.; Kudin, K. N.; Staroverov, V. N.; Kobayashi, R.; Normand, J.; Raghavachari, K.; Rendell, A.; Burant, J. C.; Iyengar, S. S.; Tomasi, J.; Cossi, M.; Rega, N.; Millam, J. M.; Klene, M.; Knox, J. E.; Cross, J. B.; Bakken, V.;

Adamo, C.; Jaramillo, J.; Gomperts, R.; Stratmann, R. E.; Yazyev, O.; Austin, A. J.; Cammi, R.; Pomelli, C.; Ochterski, J. W.; Martin, R. L.; Morokuma, K.; Zakrzewski, V. G.; Voth, G. A.; Salvador, P.; Dannenberg, J. J.; Dapprich, S.; Daniels, A. D.; Farkas, Ö.; Foresman, J. B.; Ortiz, J. V.; Cioslowski, J.; Fox, D. J. *Gaussian09*, revision D.01; Gaussian, Inc.: Wallingford, CT.

(28) Perdew, J. P.; Burke, K.; Ernzerhof, M. Generalized Gradient Approximation Made Simple. *Phys. Rev. Lett.* **1996**, *77*, 3865–3868.

(29) Rassolov, V. A.; et al. 6-31G* basis set for third-row atoms. *J. Comput. Chem.* **2001**, *22*, 976–984.

(30) Grimme, S. Semiempirical GGA-type density functional constructed with a long-range dispersion correction. *J. Comput. Chem.* **2006**, *27*, 1787–1799.

(31) (a) Gowtham, S.; Scheicher, R. H.; Pandey, R.; Karna, S. P.; Ahuja, R. First-principles study of physisorption of nucleic acid bases on small-diameter carbon nanotubes. *Nanotechnology* **2008**, *19*, No. 125701. (b) Gowtham, S.; Scheicher, R. H.; Ahuja, R.; Pandey, R.; Karna, S. P. Physisorption of nucleobases on graphene: Density-functional calculations. *Phys. Rev. B: Condens. Matter Mater. Phys.* **2007**, *76*, No. 033401.

(32) Rubio, A.; Corkill, J. L.; Cohen, M. L. Theory of graphitic boron nitride nanotubes. *Phys. Rev. B: Condens. Matter Mater. Phys.* **1994**, *49*, 5081–5084.

(33) Roman, T.; Diño, W. A.; Nakanishi, H.; Kasai, H. Amino acid adsorption on single-walled carbon nanotubes. *Eur. Phys. J. D* **2006**, *38*, 117–120.

(34) (a) Miertuš, S.; Tomasi, J. Approximate evaluations of the electrostatic free energy and internal energy changes in solution processes. *Chem. Phys.* **1982**, *65*, 239–245. (b) Tomasi, J.; Mennucci, B.; Cammi, R. Quantum mechanical continuum solvation models. *Chem. Rev.* **2005**, *105*, 2999–3093.

(35) Boys, S. F.; Bernardi, F. The calculations of small molecular interactions by the differences of separate total energies. Some procedures with reduced errors. *Mol. Phys.* **1970**, *19*, 553–566.

(36) Glendening, E. D.; Reed, A. E.; Carpenter, J. E.; Weinhold, F. *NBO*, version 3.1.